

## IMMUNOLOGY

# Fibrin gel enhances the antitumor effects of chimeric antigen receptor T cells in glioblastoma

Edikan A. Ogunnaike<sup>1,2,3</sup>, Alain Valdivia<sup>4</sup>, Mostafa Yazdimamaghani<sup>1,3</sup>, Ernesto Leon<sup>1</sup>, Seema Nandi<sup>2</sup>, Hannah Hudson<sup>1</sup>, Hongwei Du<sup>1</sup>, Simon Khagi<sup>1,5</sup>, Zhen Gu<sup>6,7</sup>, Barbara Savoldo<sup>1,8</sup>, Frances S. Ligler<sup>2,3</sup>, Shawn Hingtgen<sup>4</sup>, Gianpietro Dotti<sup>1,9\*</sup>

Regional delivery of chimeric antigen receptor (CAR) T cells in glioblastoma represents a rational therapeutic approach as an alternative to intravenous administration to avoid the blood-brain barrier impediment. Here, we developed a fibrin gel that accommodates CAR-T cell loading and promotes their gradual release. Using a model of subtotal glioblastoma resection, we demonstrated that the fibrin-based gel delivery of CAR-T cells within the surgical cavity enables superior antitumor activity compared to CAR-T cells directly inoculated into the tumor resection cavity.

## INTRODUCTION

Malignant gliomas are the most prevalent primary brain tumors, glioblastoma (GBM) being the most common and fatal (1–3). Standard therapy, based on surgical tumor resection, radiotherapy, temozolomide, and alternating electric tumor-treating fields, only delays tumor recurrence. The median survival for newly diagnosed patients remains less than 2 years (2). While resection remains critical to remove life-threatening tumor masses, novel approaches are needed to prevent tumor progression.

Immunotherapy based on the administration of checkpoint inhibitors has achieved remarkable clinical activity in many solid tumors (4). Unfortunately, this approach has been largely ineffective against GBM (5). The ineffectiveness is due, at least partly, to the paucity of endogenous infiltrating tumor-specific T cells (6, 7). The adoptive transfer of T cells redirected to target tumor-associated antigens, such as chimeric antigen receptor (CAR) T cells, represents a promising option in tumors that do not generate endogenous T cell responses (8). CAR-T cells targeting the IL13Ra2, HER2, or EGFRvIII molecules have been tested in patients with GBM, with some clinical activity documented (9–12). However, these clinical studies demonstrated that limited CAR-T cells were detected at the tumor site, highlighting the physical impediment that the blood-brain barrier (BBB) exerts on the biodistribution of CAR-T cells when these cells are infused intravenously (10–12).

The infusion of CAR-T cells into the resected tumor cavity, followed by further infusions into the ventricular system, represents the most recent approach used in clinical studies to bypass the BBB in patients with GBM (9). However, local delivery of CAR-T cells in

the resection cavity would benefit from developing innovative tools leading to optimal CAR-T cell distribution.

Fibrin is involved in the coagulation cascade, forming a physiologic clot that is critical for wound healing (13). Fibrin scaffolds have been generated, and their clinical utility relies on the fact that they are biodegradable and do not cause inflammation, tissue necrosis, or fibrosis (14). In this study, we leveraged the biocompatibility and functional properties of fibrin to create an in situ forming gel that accommodates CAR-T cells, sustains their viability, and allows their gradual release when situated within the tumor resection cavity in a GBM model. The proposed delivery system showed superior antitumor activity compared to CAR-T cells directly inoculated in the tumor resection cavity.

## RESULTS

### In situ formation of the fibrin gel

Human fibrinogen polymerized into a porous gel by enzymatic reaction with thrombin was formulated to encapsulate functional and viable T cells that can be released locally after the gel was formed in situ in the tumor resection cavity (Fig. 1A). To evaluate whether the pores distributed throughout the fibrin gel network accommodate the loading of T cells, fibrin gel was quickly formed by mixing the solution containing fibrinogen with T cells and the solution containing thrombin. The entrapment of the T cells in the pores of the cross-linked fibrin gel was confirmed using cryo-scanning electron microscopy (cryo-SEM) imaging (Fig. 1B). In addition, upon polymerization, confocal microscopy revealed that encapsulated T cells were uniformly distributed within the fluorescein-labeled fibrinogen (Fig. 1C).

Physiologic clot formation occurs in blood at the fibrinogen concentration of approximately 2 mg/ml, so we tested different concentrations of fibrin ranging from 0.3 to 5.0 mg/ml to determine the effect of fibrin density on T cell viability (15). Fibrin gels encapsulating the T cells were maintained in medium supporting T cell viability and growth for 5 days. T cell viability was evaluated daily using confocal microscopy and a two-color assay that assesses both live cells (green, green-fluorescent calcein-AM) and dead cells (red, red-fluorescent ethidium homodimer-1) based on plasma membrane integrity and esterase activity, respectively (Fig. 1D and fig. S1). The range of fibrin concentrations investigated for the gel formulation

Copyright © 2021  
The Authors, some  
rights reserved;  
exclusive licensee  
American Association  
for the Advancement  
of Science. No claim to  
original U.S. Government  
Works. Distributed  
under a Creative  
Commons Attribution  
NonCommercial  
License 4.0 (CC BY-NC).

<sup>1</sup>Lineberger Comprehensive Cancer Center, University of North Carolina, Chapel Hill, NC 27599, USA. <sup>2</sup>Joint Department of Biomedical Engineering, North Carolina State University and University of North Carolina at Chapel Hill, Raleigh, NC 27695, USA. <sup>3</sup>Center for Nanotechnology in Drug Delivery, Eshelman School of Pharmacy, University of North Carolina, Chapel Hill, NC 27599, USA. <sup>4</sup>Pharmacoengineering and Molecular Pharmaceutics, Eshelman School of Pharmacy, University of North Carolina at Chapel Hill, Chapel Hill, NC 27599, USA. <sup>5</sup>Department of Medicine, Division of Medical Oncology, University of North Carolina, Chapel Hill, NC 27599, USA. <sup>6</sup>Department of Bioengineering, University of California, Los Angeles, CA 90095, USA. <sup>7</sup>College of Pharmaceutical Sciences, Zhejiang University, Hangzhou, Zhejiang 310058, China. <sup>8</sup>Department of Pediatrics, University of North Carolina, Chapel Hill, NC 27514, USA. <sup>9</sup>Department of Microbiology and Immunology, University of North Carolina, Chapel Hill, NC 27599, USA.

\*Corresponding author. Email: gdotti@med.unc.edu

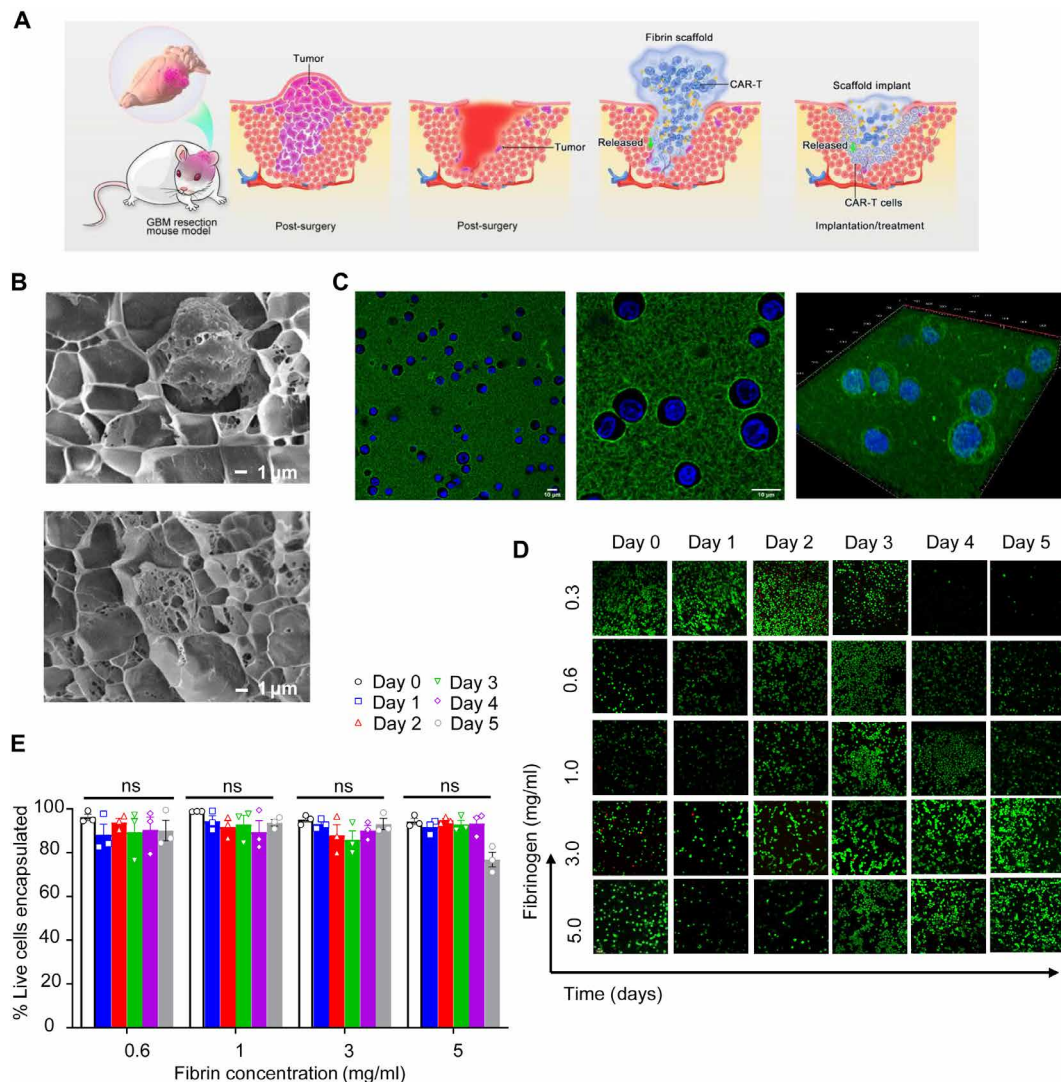


**Fig. 1. Characterization of the fibrin gel delivery system for T cells.** (A) Schematic illustration of the procedure aimed at partially removing the GBM mass and delivering CAR-T cells via fibrin gel in situ formation. The fibrin gel in the inflamed surgery site creates the matrix, allowing the gradual release of CAR-T cells. (B) Cryo-SEM imaging of the CAR-T cells within the fibrin gel. Scale bars, 1  $\mu\text{m}$ . (C) Confocal imaging of the CAR-T cells within the fibrin gel. CAR-T cells were labeled with green fluorescein, while the cell nuclei were stained with Hoechst 33254. High-resolution confocal imaging of cells encapsulated in fibrin gel is illustrated. Scale bars, 10  $\mu\text{m}$ . (D) Representative confocal imaging showing live/dead CAR-T cells encapsulated within the fibrin network for 5 days. Live cells and dead cells were labeled with green fluorescein and red fluorescein, respectively. Scale bar, 1  $\mu\text{m}$ . (E) Quantification of live CAR-T cells in the fibrin gel at different days and at different concentrations of fibrin as illustrated in (D); no difference [not significant (ns)] in viability for all concentrations.

showed no significant impact on the viability of the T cells, but T cells were retained longer in the gel with higher fibrin concentration. In contrast, fibrin formulation (0.3 mg/ml) showed loss of structural integrity over the 5-day assays and was not used for quantification (Fig. 1E). Using atomic force microscopy, we mapped murine brain tissue and compared it to the fibrin hydrogel stiffness (Fig. 2, A to F). Brain stiffness spread within the range of 20 to 80 Pa (Fig. 2A). However, we observed that the fibrin gel (0.3 mg/ml) was soft and easily contracted by the embedded cells, resulting in variable soft and stiff areas within the gel and a poor fit for the obtained data (Fig. 2B). The data suggest that the noncontracted part of the fibrin gel (0.3 mg/ml) may be relatively similar to the brain. The force map and frequency distribution graph of fibrin gels (0.3 to 5 mg/ml; Fig. 2, B to F) indicate that the moduli reported an

increase with increasing fibrinogen concentration, with brain mean at 47 Pa and gel mean moduli at 1100, 458, 411, 1533, and 2468 Pa (Fig. 2G). Overall, these data indicate that fibrin gels can be formulated to be mechanically stable and encapsulate human T cells without compromising their viability.

### Release of functional CAR-T cells from the fibrin gel

Upon establishing that fibrin gels obtained using a concentration of fibrin higher than 0.3 mg/ml are mechanically stable, we determined which density of the fibrin supports the gradual release of fully functional CAR-T cells in vitro. For these experiments, we generated CAR-T cells targeting the B7-H3 antigen (16). Specifically, we used the B7-H3-specific CAR (B7-H3) encoding the scFv obtained from the 763.73 monoclonal antibody, the stalk region of human CD8 $\alpha$ ,

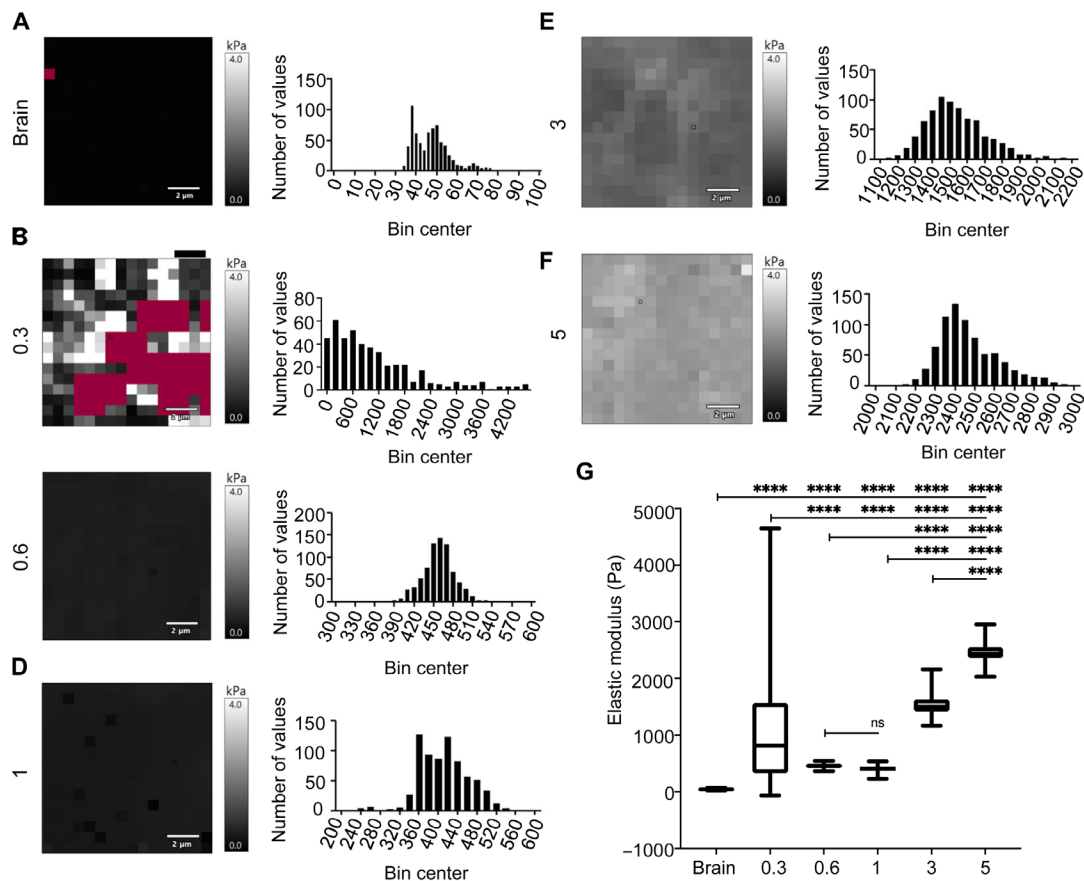


**Fig. 2. Stiffness characterization of the fibrin gel and brain tissue.** (A to F) Atomic force microscopy was performed on murine brain tissue (A) and fibrin hydrogel (0.3 to 5 mg/ml) to obtain elastic modulus measurements (B to F). (G) CAR-T cells were embedded within 200  $\mu$ l of fibrin gels formed on charged microscope slides and allowed to polymerize. Both murine brain tissue obtained from Nu/Nu mice and hydrogels were thermally equilibrated with the cantilever before taking force measurements. The overall force maps and the frequency distribution graphs are summarized, where moduli of the fibrin gels increase with increasing fibrinogen concentration. The brain moduli mean is at 47 Pa. Fibrin gels of 0.3 to 5 mg/ml recorded stiffness modulus mean at 1100, 458, 411, 1533, and 2468 Pa. \*\*\*\* $P < 0.0001$  among all groups except for 0.6 versus 1 (ns), one-way analysis of variance (ANOVA) with Tukey's post hoc.

and the CD28 and CD3 $\zeta$  chain endodomains that we previously described to exert antitumor activity in GBM (17). The CD19-specific CAR (CD19) encoding the scFv obtained from the FMC.63 monoclonal antibody, the stalk region of human CD8 $\alpha$ , and the CD28 and CD3 $\zeta$  chain endodomains was used as a negative control (18). Fibrin gels obtained using fibrin concentrations ranging from 0.3 to 5.0 mg/ml and containing T cells were seeded in cell strainers in six-well plates in complete supporting medium. Strainers were placed daily in new wells, and T cells released in the medium were counted for five consecutive days using flow cytometry and counting beads. Fibrin gels generated using fibrin (3 or 5 mg/ml) showed sustained and gradual T cell release over time (Fig. 3, A and B, and fig. S2). Of note, when CAR-T cells were labeled with carboxyfluorescein diacetate succinimidyl ester (CFSE), we observed daily CFSE dilution, indicating that CAR-T cells retain proliferative capacity when encapsulated within the fibrin gel (Fig. 3C and fig. S3). Furthermore, using 2-NBDG (2-(N-(7-Nitrobenz-2-oxa-1,3-diazol-4-yl) Amino)-2-Deoxyglucose) as a fluorescent tracer of glucose uptake into living cells, we observed that CAR-T cells uptake 2-NBDG when encapsulated in the fibrin gel. Control CAR-T cells cultured without gel and CAR-T cells encapsulated within the fibrin gel cells were collected at 60 and 120 min and evaluated by flow cytometry (Fig. 3D). Complete

uptake of 2-NBDG was observed at 120 min, suggesting that the fibrin-based gel does not compromise nutrient biodistribution (Fig. 3E). We selected the fibrin gel formulated with fibrin (3 mg/ml) for subsequent functional experiments of CAR-T cells based on these results. We first analyzed the phenotypic profile of CAR-T cells released from the fibrin gel compared to nonencapsulated CAR-T cells. CD19 CAR-T cells (F-CD19) and B7-H3 CAR-T cells (F-B7-H3) released from the fibrin gel showed expression of memory markers comparable to that of CD19 CAR-T cells and B7-H3 CAR-T cells growing in free medium (Fig. 4A). F-CD19 and F-B7-H3 CAR-T cells released from the fibrin gel were then placed in cocultures with B7-H3<sup>+</sup> GBM tumor cells (U-87 MG and U-138 MG) or CD19<sup>+</sup> tumor cells (Raji) at an effector-to-target ratio of 1:5. F-B7-H3 CAR-T cells effectively eliminated only GBM cells, and their antitumor activity was similar to that of nonencapsulated B7-H3 CAR-T cells. Control CD19 and F-CD19 CAR-T cells showed activity only against the CD19<sup>+</sup> Raji cells (Fig. 4, B and C). In addition, F-B7-H3 CAR-T cells showed superior cell counts at the end of the coculture compared to nonencapsulated B7-H3 CAR-T cells, further supporting that the fibrin gel does not impair T cell viability, proliferative capacity, and effector function (Fig. 4C). In supernatants collected from the cocultures of CAR-T cells and tumor cells, we detected interleukin-2

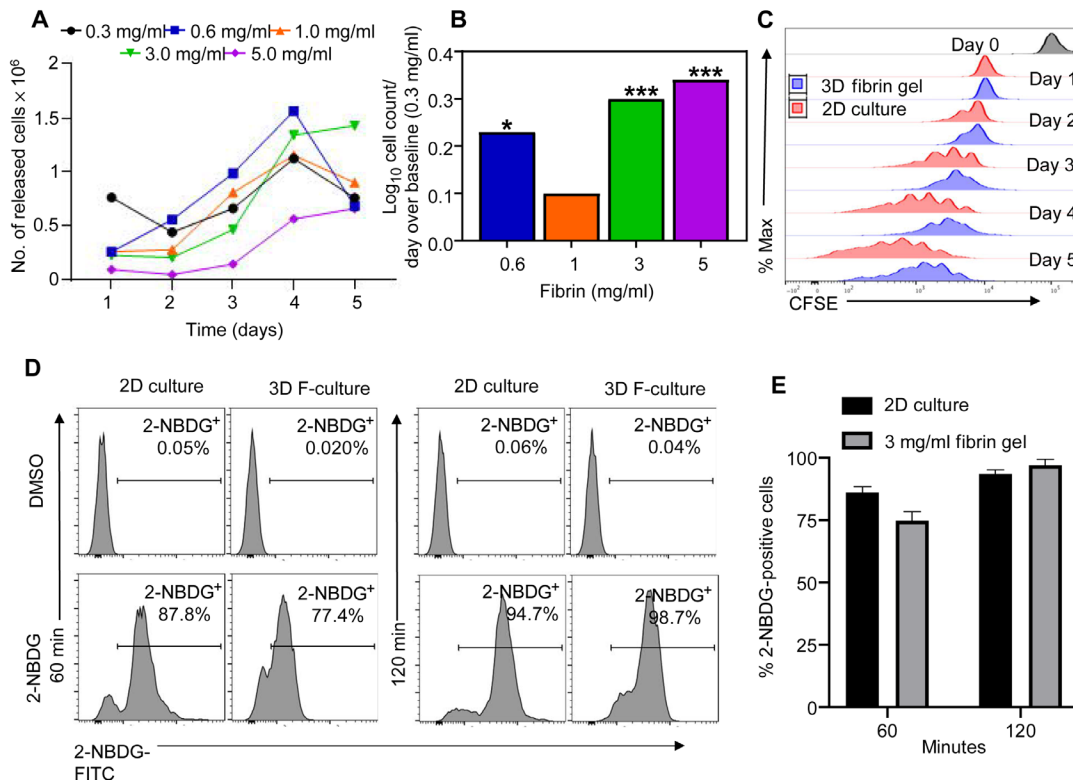


**Fig. 3. Evaluation of CAR-T cell release from the fibrin gel and glucose exchange.** (A) Representative in vitro release of T cells ( $5 \times 10^4$  cells/ml) in the fibrin gel formulated using different fibrin concentrations (0.3 to 5.0 mg/ml). Cells released from the gel were counted using flow cytometry and counting beads. (B) Summary and statistical analysis of T cell count illustrated in (A). ( $n = 5$  per each concentration). Statistical analysis was calculated as a log function of release kinetics of various concentrations of fibrinogen over days. The concentration (0.3 mg/ml) was used as the baseline. A linear model was used to fit the log of cell count as a function of released days.  $***P < 0.0001$ . (C) Representative flow cytometry plots showing the dilution of CFSE-labeled T cells encapsulated in the fibrin gel [three-dimensional (3D)] (fibrin, 3 mg/ml) and released for five consecutive days ( $n = 3$ ). CFSE-labeled T cells in liquid culture (2D) were used as control. (D) Histogram plots showing the uptake of 2-NBDG by CAR-T cells cultured in 2D and 3D at 60 and 120 min. Dimethyl sulfoxide (DMSO) was used as a control. (E) Summary of 2-NBDG uptake in 2D versus 3D as illustrated in (D).

(IL-2) and interferon- $\gamma$  (IFN- $\gamma$ ) only in response to the specific target tumor (Fig. 4D). Overall, these data indicate that CAR-T cells encapsulated and released from the fibrin gel retain their antitumor effect.

### CAR-T cells delivered via fibrin gel show antitumor activity in vivo

To assess in vivo the therapeutic effect of CAR-T cells delivered via fibrin gel, we used an image-guided tumor resection model of GBM in immunodeficient mice (Fig. 5A) (19, 20). Briefly, U-87 MG expressing green fluorescent protein (GFP)-firefly luciferase (U-87-GFP-FFLuc) were formed in situ intracranially in nude mice after performing a small craniotomy (cranial window). Twelve days later, tumors were partially resected (to mimic a minimal residual disease setting), and mice were treated by either direct intracavity inoculation of B7-H3 CAR-T cells (iC-B7-H3) or in situ formation of B7-H3 CAR-T cells within the fibrin gel (F-B7-H3) (Fig. 5B). The in situ formation of CD19 CAR-T cells within the fibrin gel (F-CD19) was used as a negative control. Tumor growth was monitored weekly by in vivo measurement of tumor bioluminescence [bioluminescence imaging (BLI)]. Control mice treated with F-CD19 CAR-T cells developed tumors rapidly and were euthanized within 15 days. Mice treated with F-B7-H3 CAR-T cells showed a significant delay in tumor growth compared to mice treated with iC-B7-H3 CAR-T cells. By day 94, 9 of the 14 (64%) mice treated with F-B7-H3 CAR-T cells

were tumor free compared to 2 of the 10 (20%) mice receiving iC-B7-H3 CAR-T cells (Fig. 5, C and D). No weight loss was observed in treated mice, ruling out concerns of toxicity (Fig. 5E). The superior control of tumor growth by F-B7-H3 CAR-T cells translated into improved survival compared to mice treated with iC-B7-H3 CAR-T cells ( $P = 0.026$ ) (Fig. 5F and fig. S4).

In separate experiments, we evaluated the degradation rate of the fibrin gel encapsulating CAR-T cells using the same model of partial tumor resection by labeling the fibrin with Alexa Fluor 647 (AF647) (Fig. 6A). Two weeks after treatment, the fluorescence signal from the gel was undetectable, and the fibrin gel was not visually detectable at necropsy, indicating the degradation of the gel (Fig. 6, B and C). We also evaluated the persistence of CAR-T cells upon delivery via direct intracavity injection or fibrin gel. For these experiments, mice were euthanized 7 to 8 days after treatment, and the brains were harvested for T cell quantification within the tumor resection area by flow cytometry (Fig. 6D). More T cells were detected in mice treated with F-B7-H3 CAR-T cells than iC-B7-H3 CAR-T cells (Fig. 6, E and F). We also performed experiments in which CAR-T cells were labeled with firefly luciferase and imaged in vivo. With the caveats of the low sensitivity of the in vivo assay, in vivo imaging also suggested improved persistence of F-B7-H3 CAR-T cells versus iC-B7-H3 CAR-T cells (fig. S5A). We did not observe significant differences in the expression of markers associated

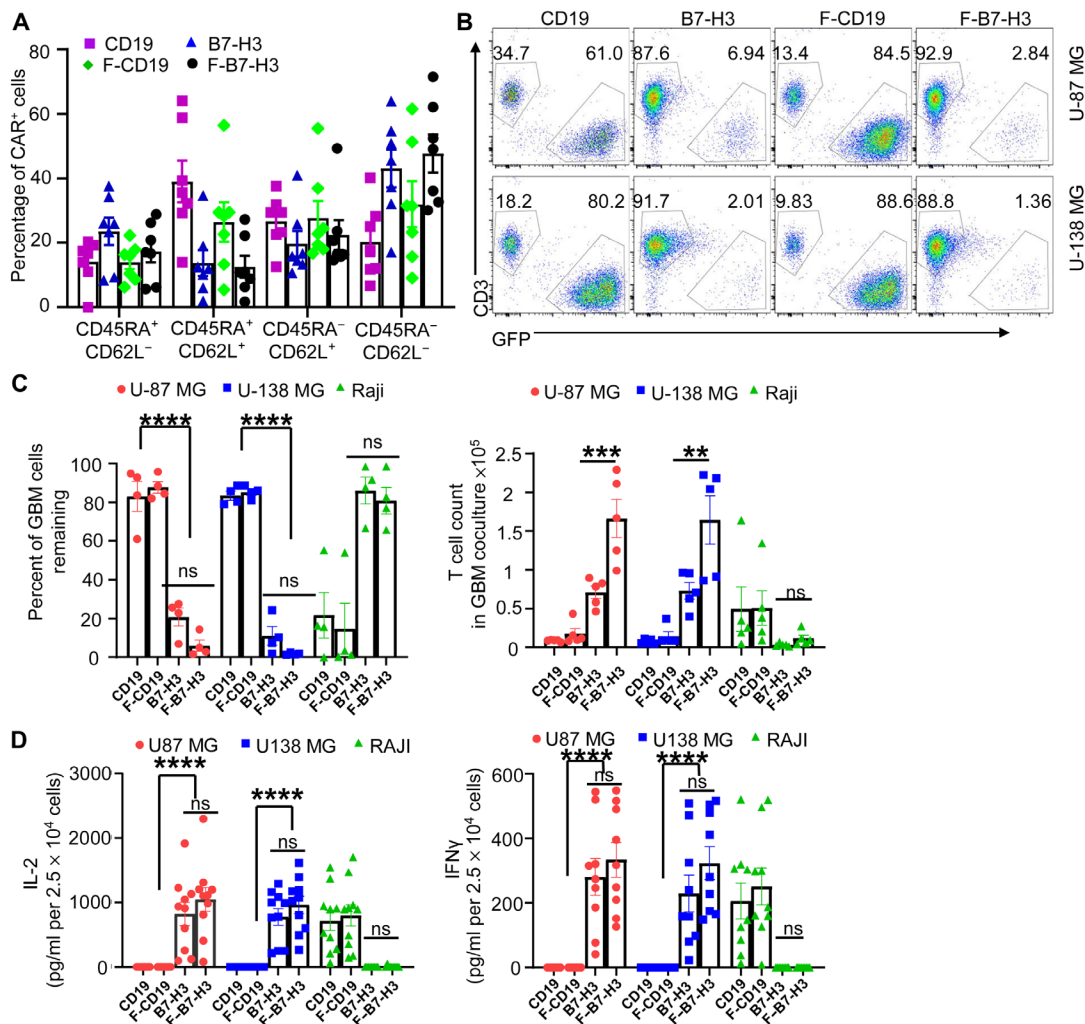


**Fig. 4. Functional characterization of CAR-T cells released from the fibrin gel.** (A) Phenotypic characterization of CD19 CAR-T cells (CD19) and B7-H3 CAR-T cells (B7-H3) growing in medium versus CD19 CAR-T cells (F-CD19) and B7-H3 CAR-T cells (F-B7-H3) released from the fibrin gel ( $n = 6$  per each condition). (B) Representative flow cytometry plots illustrating the antitumor activity of CD19, B7-H3, F-CD19, and F-B7-H3 CAR-T cells against GBM tumor cell lines U-87 MG or U-138 MG (B7-H3<sup>+</sup>) and Raji cells (CD19<sup>+</sup>) in vitro. All cells were collected on day 5 and enumerated by flow cytometry to quantify T cells (CD3<sup>+</sup>) and tumor cells (GFP<sup>+</sup>) using counting beads. (C) Quantification of tumor cells (left panel) and T cells (right panel) as described in (B) ( $n = 4-5$  per condition). \*\*\* $P = 0.0063$  against U-87 MG with 1:5 effector:target (E:T) ratio; \* $P = 0.0238$  against U-138 MG with a 1:5 E:T ratio; \*\*\*\* $P < 0.0001$  and \*\*\*\* $P < 0.0006$  for B7-H3 and F-B7-H3, respectively, determined by repeated measurement of two-way ANOVA with Turkey's multiple comparison test. (D) Quantification of IL-2 (left panel) and IFN- $\gamma$  (right panel) in the supernatant of the cocultures described in (B) ( $n = 9$  per condition). \*\*\*\* $P < 0.0001$  for CD19 and F-CD19 control against B7-H3 and F-B7-H3, respectively, determined by two-way ANOVA using Turkey's multiple comparisons test.

with exhaustion and memory, like PD1 and CD62L, respectively, in tumor-infiltrating T cells (Fig. 6G). However, the number of tumor-infiltrating CD3<sup>+</sup> T cells positively correlated with lower numbers of tumor cells at the time of tumor harvest in tumor-bearing mice treated with F-B7-H3 CAR-T cells (fig. S5B). Overall, these data indicate that fibrin gel-assisted delivery of CAR-T cells improves the antitumor effects of CAR-T cells in a tumor model of GBM by promoting the persistence of these cells.

**DISCUSSION**

In this study, bioactive fibrin was used to obtain a biocompatible gel that accommodates CAR-T cells and can be formed in situ in the resection cavity upon surgical removal of the GBM tumor mass. We

observed that the regional administration of CAR-T cells via fibrin gel is superior in controlling local tumor growth compared to the inoculation of free CAR-T cells in the resection cavity.

Local delivery of CAR-T cells is a clinically appealing strategy for the treatment of malignancies characterized by predominant regional growth and recurrence such as primary brain tumors, retinoblastoma, or intrapleural or intraperitoneal malignancies (9, 21, 22). However, the direct inoculation of the CAR-T cells into the cavity remaining after surgery inevitably requires optimization. Effective local delivery of CAR-T cells must ensure the broad coverage of the surface of the resection cavity to maximize the possibility that T cells enter in contact with residual tumor cells. Therefore, we hypothesized that a mechanically flexible scaffold could adapt to the resection cavity of the tumor, allowing ample biodistribution of the

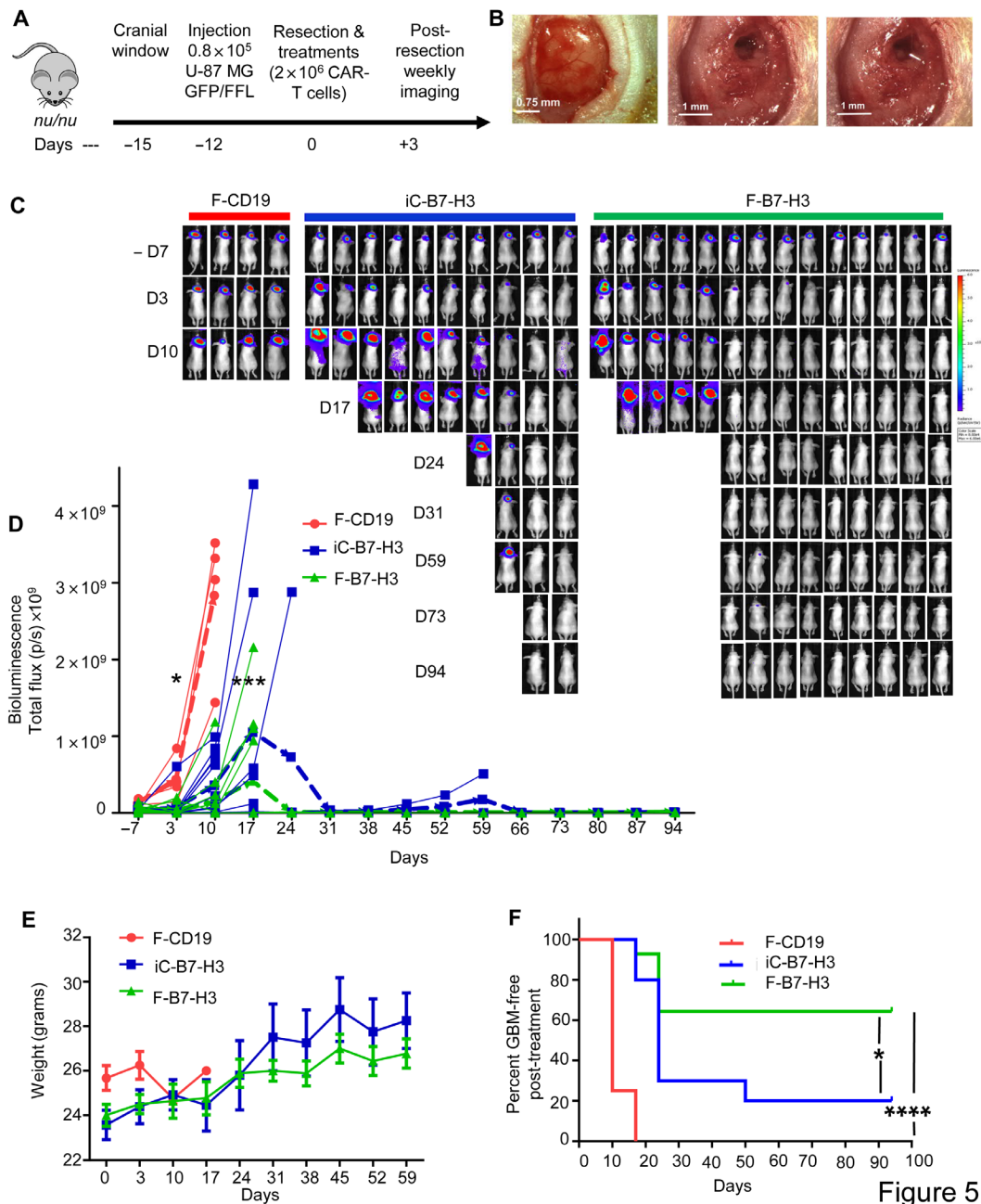


Figure 5

**Fig. 5. CAR-T cells delivered via fibrin gel control GBM tumor growth after partial resection.** (A) Schematic of the xenograft GBM model in which the tumor mass is partially resected and mice are treated with CAR-T cells inoculated via direct intracavity injection (iC-B7-H3) or by in situ formation of the fibrin gel (F-B7-H3). Control mice received CD19 CAR-T cells encapsulated in the fibrin gel (F-CD19). (B) Representative images showing tumor before resection (left panel), after surgery (middle panel), and after fibrin gel formed in situ in the tumor resection cavity (right panel). Scale bar, 0.75 mm - 1 mm. (C) Representative tumor BLI images showing tumor growth in F-CD19-, iC-B7-H3-, and F-B7-H3-treated mice. (D) Tumor BLI kinetics in F-CD19-, iC-B7-H3-, and F-B7-H3-treated mice (4 to 15 mice per group). \* $P=0.0296$  and  $0.0471$  for day -7 and day 3 versus day 17 in iC-B7-H3 versus F-B7-H3, (blue bold dotted line and green bold dotted line, indicating the averages respectively), determined by Turkey's multiple comparison test; \*\*\* $P=0.0009$  as overall function calculated by two-way ANOVA. (E) Quantification of mouse weight in the experimental groups described in (B). (F) Kaplan-Meier survival curve of the treated mice as described in (C). \* $P=0.0259$  (iC-B7-H3 versus F-B7-H3); \*\*\*\* $P<0.0001$  (F-CD19 versus F-B7-H3),  $\chi^2$  test. For the survival curve, mice were censored when the BLI signal reached  $1 \times 10^9$  photons per second. Photo credit: E. A. Ogunnaike, University of North Carolina, Chapel Hill.

CAR-T cells. In addition, the scaffold should guarantee the integrity and functionality of these CAR-T cells.

Biocompatible fibrin gels exhibit excellent biodegradability and wound healing properties and are used for many applications, including hemostatic balance, regenerative medicine, and drug

delivery (23–26). We leveraged the ability of fibrin to assemble rapidly through the activation of fibrinogen by thrombin in a calcium-containing buffer and generated a mechanically stable gel that holds CAR-T cells. The gel is porous and allows complete and gradual CAR-T cell releases from the matrix. When accommodated within

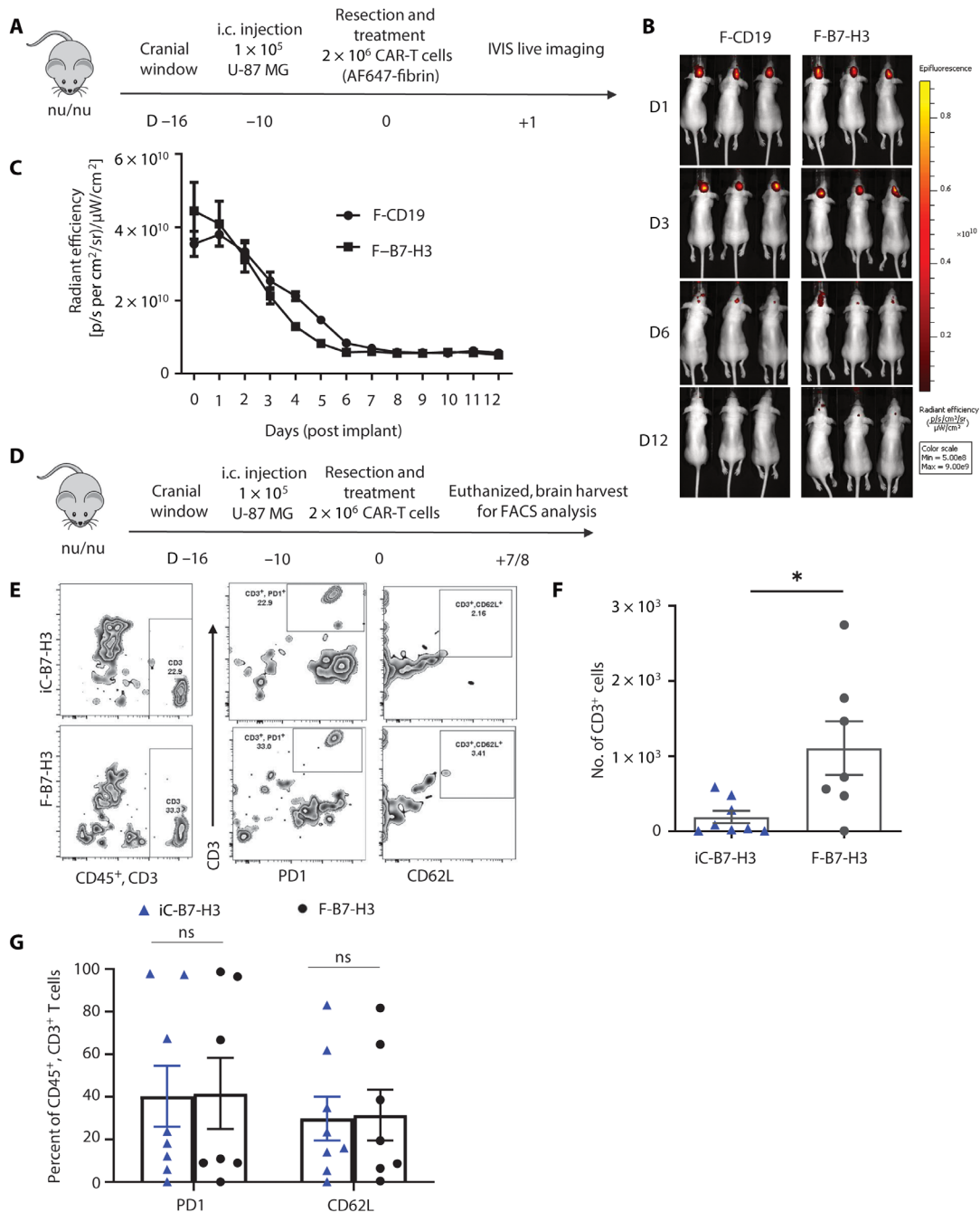


**Fig. 6. Degradation of fibrin gel and CAR-T cell persistence in vivo.** (A) Schematic of the murine xenograft model of partial tumor resection to assess the degradation of the fibrin gel encapsulating CD19 CAR-T cells (F-CD19) or B7-H3 CAR-T cells (F-B7-H3). Fibrin was labeled with 647, and fluorescence of the fibrin was imaged daily. i.c., intracranially. (B) Representative fluorescence image signal of the fibrin gel. (C) Quantification of the fibrin gel degradation in the model described in (A) ( $n = 5$  per group). (D) Schematic of the murine xenograft model of partial tumor resection to assess CAR-T cell persistence. After partial tumor resection, mice were then randomized to receive B7-H3 CAR-T cells inoculated via direct intracavity injection (iC-B7-H3) or via the fibrin gel (F-B7-H3). Mice were euthanized 7 to 8 days after treatment, and brains were harvested to detect CAR-T cells by flow cytometry. FACS, fluorescence-activated cell sorting. (E and F) Representative flow cytometry plots (E) and counts of CD3<sup>+</sup>T cells using counting beads (F) detected at days 7 and 8 upon iC-B7-H3 or F-B7-H3 CAR-T cells.  $P = 0.0190$  ( $n = 7$  per group). (G) Flow cytometry quantification using counting beads of CD3<sup>+</sup>PD1<sup>+</sup> and CD3<sup>+</sup>CD62L<sup>+</sup> T cells detected at days 7 and 8 after upon iC-B7-H3 or F-B7-H3 CAR-T cells.  $n = 7-8$  per group.

the resection cavity, the fibrin solution containing CAR-T cells forms the fibrin gel quickly in situ upon local addition of thrombin. Using this strategy, CAR-T cells can receive nutrients within the fibrin gel, which is critical for their survival, and remain fully functional

when released from the gel. In addition, we demonstrated improved antitumor activity of CAR-T cells when delivered via the fibrin gel compared to inoculation of the same CAR-T cells within the tumor resection cavity. Furthermore, it has been previously demonstrated

that fibrin-treated wounds have an increased number of CD31-positive endothelial cells and hemostatic properties (13). Thus, we did not observe delays in the healing process when fibrin-based delivery of CAR-T cells was used.

Collectively, these results suggest that regional delivery of CAR-T cells encapsulated in a fibrin gel may provide antitumor activity over an extended period of time after surgery in patients. The proposed intracavity treatment may also be combined with the subsequent administration of CAR-T cells via intraventricular administration, as currently adopted in pilot clinical studies to further extend the distribution of the CAR-T cells. Furthermore, the fibrin gel would allow the possibility to load and locally deliver cytokines and biological agents, additionally sustaining T cell growth and countering immunosuppressive tumor-associated mechanisms.

## MATERIALS AND METHODS

### Cell lines and cell culture

Human B cell lymphoma Raji (source: male) and GBM tumor cell line U-87 MG (source: male) [Research Resource Identifiers (#RRID): CVCL\_0022] were obtained from the American Type Culture Collection (ATCC), and U-138 MG cells (RRID: CVCL\_0020) were obtained from Leibniz Institute DSMZ - German Collection of Microorganisms and Cell Cultures GmbH. Cells were grown in RPMI 1640 or Dulbecco's modified Eagle's medium (Thermo Fisher Scientific) supplemented with 10% fetal bovine serum (FBS) (Gemini Bio Products), 1% penicillin/streptomycin (Thermo Fisher Scientific), and 1% GlutaMAX (Thermo Fisher Scientific). The SFG retroviral vector encoding GFP and firefly luciferase genes (SFG.GFP-FFLuc) was used to generate dual GFP- and FFLuc-expressing cell lines (17). Cells were maintained in a humidified atmosphere containing 5% CO<sub>2</sub> at 37°C. Cell lines were routinely tested to confirm the absence of mycoplasma and for the expression of the targeted antigen by flow cytometry.

### Formation and characterization of CAR-T cells in the fibrin gel

Fibrin gels were obtained by mixing 10:1 volume of fibrinogen depleted of plasminogen, von Willebrand factor, and fibronectin FIB3 (Enzyme Research Laboratories, South Bend, IN) and thrombin (1 NIH U ml<sup>-1</sup>) and HT 1002a (Enzyme Research Laboratories, South Bend, IN) in Hepes buffer (25 mM Hepes, 150 mM NaCl, and 5 mM CaCl<sub>2</sub>; pH 7.4). All functional assays were assessed using fibrinogen (3 mg/ml) reacted with thrombin (1 U/ml). CAR-T cells (1 × 10<sup>5</sup> cells) were encapsulated in the fibrin gel, embedded with optimal cutting temperature (OCT), and immersed in liquid nitrogen. The morphology of the F-CAR-T cells was characterized by cryo-SEM (JEOL 7600F, Gatan Alto). The encapsulation of CAR-T cells in fibrin was further characterized by confocal microscopy (Zeiss LSM 710). Alexa Fluor 488 (AF488)-fibrinogen was purchased from Thermo Fisher Scientific.

### Retrovirus preparation and transduction and expansion of human T cells

Retroviral supernatants used for the transduction of human T cells were prepared as previously described (27). Briefly, 293T cells (2 × 10<sup>6</sup>) were seeded in a 10-cm cell culture dish and transfected with the plasmid mixture of the retroviral vector, the Peg-Pam-e plasmid encoding MoMLV gag-pol, and the RDF plasmid encoding

the RD114 envelope using transfection reagents. The supernatant was collected 48 and 72 hours after transfection and filtered with 0.45-μm filters. For the generation of CAR-T cells, buffy coats from healthy donors were purchased from the Gulf Coast Regional Blood Center (Houston, TX). Peripheral blood mononuclear cells isolated with Lymphoprep density separation (Fresenius Kabi Norge) were activated with immobilized CD3 (Miltenyi Biotec) and CD28 (BD Biosciences) antibodies and then transduced with retroviral supernatants on retronectin-coated plates (Takara Bio Inc., Shiga, Japan). T cells were subsequently expanded in complete medium [45% RPMI 1640, 45% Click's medium (Irvine Scientific), 10% FBS (HyClone), 2 mM GlutaMAX, penicillin (100 U/ml), and streptomycin (100 μg/ml)] supplemented with IL-7 (10 ng/ml; PeproTech) and IL-15 (5 ng/ml; PeproTech). T cells were used for in vitro and in vivo analyses on days 12 to 14. Two days before in vitro functional evaluation, cells were plated in cytokine-free medium (28, 29).

### Confocal microscopic imaging

To visualize the distribution of cells in the fibrin gel (AF488-fibrin), CAR-T cells were labeled with Hoechst 33254. CAR-T cells (1 × 10<sup>6</sup> cells) were polymerized in the hydrogel and immersed in culture medium using MatTek microwell dishes and analyzed by confocal microscope. To qualitatively and quantitatively characterize the viability and proliferation of CAR-T cells in the fibrin gel matrix and assess the morphology of T cells interacting with the matrix, we used a Zeiss LSM 710 inverted confocal microscope with differential interference contrast (DIC) controlled by Zeiss ZEN 2011 software. CAR-T cells (1 × 10<sup>6</sup>) were polymerized in the fibrin gel and placed in culture medium. Cells in the fibrin gel were analyzed for viability on days 1 to 5, in which cells were stained by immersing the hydrogel in the LIVE/DEAD Viability/Cytotoxicity Kit for 10 min. Samples were analyzed with a confocal microscope, where live cells were labeled with green fluorescein and dead cells with red fluorescein. The Imaris image visualization and analysis software (Oxford Instruments) was used on at least three different Z-stack slices to quantify the number of live and dead cells for each sample.

### Enzyme-linked immunosorbent assay

T cells (0.2 × 10<sup>5</sup>) were cocultured with tumor cells (1 × 10<sup>5</sup>) in 24-well plates without the addition of exogenous cytokines. After 24 hours, the supernatants were collected, and cytokines (IFN-γ and IL-2) were measured in duplicate using specific enzyme-linked immunosorbent assay (ELISA) kits (R&D Systems) following the manufacturer's instructions. T cells were encapsulated and released from the fibrin scaffold before being cocultured with tumor cells.

### Flow cytometry

We performed flow evaluations using antibodies specific to human CD3, CD4, CD8, CD19, CD27, CD45, CD45RA, CD62L, CCR7, B7-H3, PD-1, PD-L1, and TIM3 and murine CD3, CD4, CD8, CD11b, CD11c, PD-1, and Ly-6G (from BD Biosciences and BioLegend) conjugated with BV421, BV510, BV605, BV711, fluorescein isothiocyanate (FITC), AF488, peridinin chlorophyll protein (PerCP)-cy5.5, phycoerythrin (PE), PE-cy7, allophycocyanin (APC), and APC-cy7 fluorochromes. Expression of human B7-H3 by tumor cell lines was assessed with the 376.96 monoclonal antibody and confirmed with the commercial B7-H3 antibody clone 7-517 (BD Biosciences) (16). Expression of B7-H3.CAR was evaluated using the fusion protein 2Ig-B7-H3-GFP. Samples were acquired with BD

FACSCanto II or BD LSRFortessa using the BD FACSDiva software (BD Biosciences). Quantification and characterization of T cells within the tumor were obtained by generating single-cell suspension of the tissues using the Human Tumor Dissociation Kit (Miltenyi Biotec) as per the manufacturer's instructions. For each sample, a minimum of 10,000 events was acquired, and data were analyzed using FlowJo version 10.

### Coculture and T cell proliferation assays

Tumor cells were seeded in 24-well plates at a concentration of  $1 \times 10^5$  cells per well. T cells were added to the culture at different ratios (effector:target of 1:1 or 1:5) without the addition of exogenous cytokines. T cells encapsulated in fibrin gel were released for 3 days and then collected and used for all cocultures as F-CAR-T cells. Cells were analyzed on days 5 to 7 to measure residual tumor cells and T cells by flow cytometry (17). Zombie Aqua Dye (BioLegend) was used to gate on viable cells. T cells were identified by the expression of CD3 and tumor cells by GFP expression (U-87 MG and U-138 MG) or CD19 (Raji). T cells were labeled with 1.5 mM CFSE (Invitrogen) and encapsulated in a fibrin scaffold to assess proliferation. CFSE dilution was measured on gated T cells released from the gel each day for 5 days (17).

### Atomic force microscopy

The elastic moduli of fibrin gels were measured using an atomic force microscope (AFM) (MFP-3D-BIO, Asylum Research) in contact force mode using silicon nitride cantilevers (NanoAndMore) with a particle diameter of 1.98  $\mu\text{m}$ . The spring constant of each cantilever was determined using the AFM software (IGOR Pro 16). CAR-T cells were embedded within 200  $\mu\text{l}$  of fibrin gels (0.3 to 5 mg/ml) formed on charged microscope slides. Murine brain tissue was obtained from Nu/Nu mice and thermally equilibrated with the cantilever in  $1 \times$  phosphate-buffered saline (PBS) for 30 min before taking force measurements. Fibrin gels were first allowed to polymerize on microscope slides for 1 hour and then thermally equilibrated with the cantilever in  $1 \times$  PBS for 30 min before taking force measurements. Force maps, each consisting of 256 individual force curves, were obtained for three  $10 \mu\text{m} \times 10 \mu\text{m}$  randomly chosen areas of each sample. Each force map was fitted by applying the Hertz model to the linear region of the force curve to obtain the modulus of the sample.

### Xenogeneic mouse model

Mouse experiments were approved by the Institutional Animal Care and Use Committee of University of North Carolina. A small circular window in the skull was made using a bone drill (Ideal Micro Drill, Harvard Apparatus, Holliston, MA), exposing the right frontal lobe of the brain of 6- to 10-week-old nude female mice (19). One week later, FFluc-U-87 MG tumor cells were suspended in 5  $\mu\text{l}$  of PBS and inoculated in the brain using a Hamilton syringe, approximately 1 mm deep. Twelve days after tumor inoculation, a surgical resection cavity was made by removing roughly 90% of the engrafted tumor. Bleeding was controlled with the hemostatic agent (SURGICEL, Ethicon, Somerville, NJ) and rinsed with cold saline. For intracranial delivery, CAR-T cells ( $2 \times 10^6$  cells per mouse) were resuspended in PBS and injected into the resection cavity using a p10 pipette in a volume of 3  $\mu\text{l}$ , which was equivalent to the fibrin gel volume CAR-T cells. We previously demonstrated that  $2 \times 10^6$  CAR-T cells per mouse could provide antitumor effects when inoculated directly intratumorally

(17, 30). For the fibrin gel-mediated delivery, CAR-T cells were formed in situ in the cavity by inoculating fibrin solution with CAR-T cells and immediately adding thrombin solution for a concentration of 3 mg/ml of F-CAR-T cells in 3- $\mu\text{l}$  volume intracavity. The incision was closed with Vetbond Tissue Adhesive (3M, Maplewood, MN). For pain management, meloxicam (5 mg/kg) was administered subcutaneously before and after surgery once a day for 3 days. Tumor growth was monitored by BLI (PerkinElmer IVIS Lumina In Vivo Imaging System) weekly. Mice were euthanized when showing signs of discomfort according to veterinary recommendation and animal protocol. To assess the persistence/degradation of the fibrin-based gel, we used the same model described above with fibrin labeled with AF647. Fluorescence was measured noninvasively in the brain over time using the PerkinElmer IVIS Lumina In Vivo Imaging System (Waltham, MA) at excitation 710 to 760 nm and emission 810 to 875 nm with 1- to 10-s exposure times. Total flux ( $\rho/\text{s}$ ) values from each mouse were normalized to the total flux from day 0.

### Statistical analysis

All results are presented as means  $\pm$  SEM, as indicated. Tukey post hoc tests and one-way analysis of variance (ANOVA) were used for multiple comparisons (when more than two groups were compared), and Student's *t* test was used for two-group comparisons. The survival benefit was determined using a log-rank test. All statistical analyses were carried out with the Prism software package (PRISM 5.0; GraphPad Software, 2007).

### SUPPLEMENTARY MATERIALS

Supplementary material for this article is available at <https://science.org/doi/10.1126/sciadv.abg5841>

[View/request a protocol for this paper from Bio-protocol.](#)

### REFERENCES AND NOTES

- H. S. Friedman, M. D. Prados, P. Y. Wen, T. Mikkelsen, D. Schiff, L. E. Abrey, W. K. A. Yung, N. Paleologos, M. K. Nicholas, R. Jensen, J. Vredenburgh, J. Huang, M. Zheng, T. Cloughesy, Bevacizumab alone and in combination with irinotecan in recurrent glioblastoma. *J. Clin. Oncol.* **27**, 4733–4740 (2009).
- R. J. Komotar, M. L. Otten, G. Moise, E. S. Connolly, Radiotherapy plus concomitant and adjuvant temozolomide for glioblastoma—A critical review. *Clin. Med. Oncol.* **2**, 421–422 (2008).
- M. Weller, N. Butowski, D. D. Tran, L. D. Recht, M. Lim, H. Hirte, L. Ashby, L. Mechtler, S. A. Goldlust, F. Iwamoto, J. Drappatz, D. M. O'Rourke, M. Wong, M. G. Hamilton, G. Finocchiaro, J. Perry, W. Wick, J. Green, Y. He, C. D. Turner, M. J. Yellin, T. Keler, T. A. Davis, R. Stupp, J. H. Sampson, J. Campian, K. Becker, G. Barnett, G. Nicholas, A. Desjardins, T. Benkers, N. Wagle, M. Groves, S. Kesari, Z. Horvath, R. Merrell, R. Curry, J. O'Rourke, D. Schuster, M. Mrugala, R. Jensen, J. Trusheim, G. Lesser, K. Belanger, A. Sloan, B. Puroo, K. Fink, J. Raizer, M. Schuler, S. Nair, S. Peak, A. Brandes, N. Mohile, J. Landolfi, J. Olson, R. Jennens, P. DeSouza, B. Robinson, M. Crittenden, K. Shih, A. Flowers, S. Ong, J. Connelly, C. Hadjipanayis, P. Giglio, F. Mott, D. Mathieu, N. Lessard, S. J. Sepulveda, J. Lövey, H. Wheeler, P. L. Inglis, C. Hardie, D. Bota, M. Lesniak, J. Portnow, B. Frankel, L. Junck, R. Thompson, L. Cher, E. McGhie, D. Macdonald, F. Saran, R. Soffietti, D. Blumenthal, S. B. C. M. André de, A. Nowak, N. Singhal, A. Hottinger, A. Schmid, G. Srkalovic, D. Baskin, C. Fadul, L. Nabors, R. LaRocca, J. Villano, N. Paleologos, P. Kavan, M. Pitz, B. Thiessen, A. Idhah, J. S. Frenel, J. Dumont, O. Grauer, P. Hau, C. Marosi, J. P. Dühr, S. Shao, H. Ashamalla, M. Weaver, J. Lutzky, N. Avgeropoulos, W. Hanna, M. Nadipuram, G. Cecchi, R. O'Donnell, S. Pannullo, J. Carney, M. MacNeil, R. Beaney, M. Fabbro, O. Schnell, R. Fietkau, G. Stockhammer, B. Malinova, K. Odrzask, M. Sames, G. M. Gil, E. Razis, K. Lavrenkov, G. Castro, F. Ramirez, C. Baldotto, F. Viola, S. Malheiros, J. Lickliter, S. Gauden, A. Dechaphunkul, I. Thaipaisuttikul, Z. Thothathil, H. I. Ma, W. Y. Cheng, C. H. Chang, F. Salas, P. Y. Dietrich, C. Mamot, L. Nayak, S. Nag, Rindopepimut with temozolomide

- for patients with newly diagnosed, EGFRvIII-expressing glioblastoma (ACT IV): A randomised, double-blind, international phase 3 trial. *Lancet Oncol.* **18**, 1373–1385 (2017).
4. J. Larkin, V. Chiarion-Sileni, R. Gonzalez, J. J. Grob, C. L. Cowey, C. D. Lao, D. Schadendorf, R. Dummer, M. Smylie, P. Rutkowski, P. F. Ferrucci, A. Hill, J. Wagstaff, M. S. Carlino, J. B. Haanen, M. Maio, I. Marquez-Rodas, G. A. McArthur, P. A. Ascierto, G. V. Long, M. K. Callahan, M. A. Postow, K. Grossman, M. Sznol, B. Dreno, L. Bastholt, A. Yang, L. M. Rollin, C. Horak, F. S. Hodi, J. D. Wolchok, Combined nivolumab and ipilimumab or monotherapy in untreated melanoma. *N. Engl. J. Med.* **373**, –23, 34 (2015).
  5. D. A. Reardon, A. A. Brandes, A. Omuro, P. Mulholland, M. Lim, A. Wick, J. Baehring, M. S. Ahluwalia, P. Roth, O. Bähr, S. Phuphanich, J. M. Sepulveda, P. De Souza, S. Sahebjam, M. Carleton, K. Tatsuoka, C. Taitt, R. Zwiertes, J. Sampson, M. Weller, Effect of nivolumab vs bevacizumab in patients with recurrent glioblastoma: The CheckMate 143 phase 3 randomized clinical trial. *JAMA Oncol.* **6**, 1003–1010 (2020).
  6. D. A. Reardon, J. H. Sampson, S. Sahebjam, M. Lim, J. M. Baehring, G. Vlahovic, T. F. Cloughesy, L. C. Strauss, R. R. Latek, P. Paliwal, C. T. Harbison, A. D. Voloschin, A. M. P. Omuro, Safety and activity of nivolumab (nivo) monotherapy and nivo in combination with ipilimumab (ipi) in recurrent glioblastoma (GBM): Updated results from checkmate-143. *J. Clin. Oncol.* **34**, 2014 (2016).
  7. M. D. Iglesias, J. S. Parker, K. A. Hoadley, J. S. Serody, C. M. Perou, B. G. Vincent, Genomic analysis of immune cell infiltrates across 11 tumor types. *J. Natl. Cancer Inst.* **108**, djw144 (2016).
  8. G. Fuca, L. Reppel, E. Landoni, B. Savoldo, G. Dotti, Enhancing chimeric antigen receptor t-cell efficacy in solid tumors. *Clin. Cancer Res.* **26**, 2444–2451 (2020).
  9. C. E. Brown, D. Alizadeh, R. Starr, L. Weng, J. R. Wagner, A. Naranjo, J. R. Ostberg, M. S. Blanchard, J. Kilpatrick, J. Simpson, A. Kurien, S. J. Priceman, X. Wang, T. L. Harshbarger, M. D'Apuzzo, J. A. Ressler, M. C. Jensen, M. E. Barish, M. Chen, J. Portnow, S. J. Forman, B. Badie, Regression of glioblastoma after chimeric antigen receptor T-cell therapy. *N. Engl. J. Med.* **375**, 2561–2569 (2016).
  10. D. M. O'Rourke, M. P. Nasrallah, A. Desai, J. J. Melenhorst, K. Mansfield, J. J. D. Morrisette, M. Martinez-Lage, S. Brem, E. Maloney, A. Shen, R. Isaacs, S. Mohan, G. Plesa, S. F. Lacey, J. M. Navenot, Z. Zheng, B. L. Levine, H. Okada, C. H. June, J. L. Brogdon, M. V. Maus, A single dose of peripherally infused EGFRvIII-directed CAR T cells mediates antigen loss and induces adaptive resistance in patients with recurrent glioblastoma. *Sci. Transl. Med.* **9**, eaaa0984 (2017).
  11. S. L. Goff, R. A. Morgan, J. C. Yang, R. M. Sherry, P. F. Robbins, N. P. Restifo, S. A. Feldman, Y. C. Lu, L. Lu, Z. Zheng, L. Xi, M. Epstein, L. S. McIntyre, P. Malekzadeh, M. Raffeld, H. A. Fine, S. A. Rosenberg, Pilot trial of adoptive transfer of chimeric antigen receptor-transduced t cells targeting egfrviii in patients with glioblastoma. *J. Immunother.* **42**, 126–135 (2019).
  12. N. Ahmed, V. Brawley, M. Hegde, K. Bielamowicz, M. Kalra, D. Landi, C. Robertson, T. L. Gray, O. Diouf, A. Wakefield, A. Ghazi, C. Gerken, Z. Yi, A. Ashoori, M. F. Wu, H. Liu, C. Rooney, G. Dotti, A. Gee, J. Su, Y. Kew, D. Baskin, Y. J. Zhang, P. New, B. Grilley, M. Stojakovic, J. Hicks, S. Z. Powell, M. K. Brenner, H. E. Heslop, R. Grossman, W. S. Wels, S. Gottschalk, HER2-specific chimeric antigen receptor–modified virus-specific T cells for progressive glioblastoma: A phase 1 dose-escalation trial. *JAMA Oncol.* **3**, 1094–1101 (2017).
  13. C. Cam, S. Zhu, N. F. Truong, P. O. Scumpia, T. Segura, Systematic evaluation of natural scaffolds in cutaneous wound healing. *J. Mater. Chem. B* **3**, 7986–7992 (2015).
  14. M. R. Jackson, New and potential uses of fibrin sealants as an adjunct to surgical hemostasis. *Am. J. Surg.* **182**, 36–39 (2001).
  15. I. V. Kaplan, M. Attaelmannan, S. S. Levinson, Fibrinogen is an antioxidant that protects  $\beta$ -lipoproteins at physiological concentrations in a cell free system. *Atherosclerosis* **158**, 455–463 (2001).
  16. H. Du, K. Hirabayashi, S. Ahn, N. P. Kren, S. A. Montgomery, X. Wang, K. Tiruthani, B. Mirlekar, D. Michaud, K. Greene, S. G. Herrera, Y. Xu, C. Sun, Y. Chen, X. Ma, C. R. Ferrone, Y. Pylayeva-Gupta, J. J. Yeh, R. Liu, B. Savoldo, S. Ferrone, G. Dotti, Antitumor responses in the absence of toxicity in solid tumors by targeting B7-H3 via chimeric antigen receptor T cells. *Cancer Cell* **35**, 221–237.e8 (2019).
  17. D. Nehama, N. Di Ianni, S. Musio, H. Du, M. Patané, B. Pollo, G. Finocchiaro, J. J. H. Park, D. E. Dunn, D. S. Edwards, J. S. Damrauer, H. Hudson, S. R. Floyd, S. Ferrone, B. Savoldo, S. Pellegatta, G. Dotti, B7-H3-redirected chimeric antigen receptor T cells target glioblastoma and neurospheres. *EBioMedicine* **47**, 33–43 (2019).
  18. C. Sun, P. Shou, H. Du, K. Hirabayashi, Y. Chen, L. E. Herring, S. Ahn, Y. Xu, K. Suzuki, G. Li, O. Tshouridis, L. Su, B. Savoldo, G. Dotti, THEMIS-SHP1 recruitment by 4-1BB tunes LCK-mediated priming of chimeric antigen receptor-redirected T cells. *Cancer Cell* **37**, 216–225.e6 (2020).
  19. K. T. Sheets, J. R. Bagó, I. L. Paulk, S. D. Hingtgen, Image-guided resection of glioblastoma and intracranial implantation of therapeutic stem cell-seeded scaffolds. *J. Vis. Exp.* **2018**, 2018, 5742
  20. S. Suryaprakash, Y. H. Lao, H. Y. Cho, M. Li, H. Y. Ji, D. Shao, H. Hu, C. H. Quek, D. Huang, R. L. Mintz, J. R. Bagó, S. D. Hingtgen, K. B. Lee, K. W. Leong, Engineered mesenchymal stem cell/nanomedicine spheroid as an active drug delivery platform for combinational glioblastoma therapy. *Nano Lett.* **19**, 1701–1705 (2019).
  21. P. S. Adusumilli, M. G. Zauderer, V. W. Rusch, R. O'Ceirbhail, A. Zhu, D. Ngai, E. McGee, N. Chintala, J. Messinger, W. Cheema, E. Halton, C. Diamonte, J. Pineda, A. Vincent, S. Modi, S. B. Solomon, D. R. Jones, R. Brentjens, I. Riviere, M. Sadelain, Regional delivery of mesothelin-targeted CAR T cells for pleural cancers: Safety and preliminary efficacy in combination with anti-PD-1 agent. *J. Clin. Oncol.* **37**, 2511 (2019).
  22. K. Wang, Y. Chen, S. Ahn, M. Zheng, E. Landoni, G. Dotti, B. Savoldo, Z. Han, C. Hill, C. Hill, C. Hill, C. Hill, C. Hill, GD2-specific CAR T cells encapsulated in an injectable hydrogel control retinoblastoma and preserve vision. *Nat. Cancer* **1**, 990–997 (2020).
  23. B. Bujoli, J. C. Scimeca, E. Verron, Fibrin as a multipurpose physiological platform for bone tissue engineering and targeted delivery of bioactive compounds. *Pharmaceutics* **11**, 1–15 (2019).
  24. P. A. Janmey, J. P. Winer, J. W. Weisel, Fibrin gels and their clinical and bioengineering applications. *J. R. Soc. Interface* **6**, 1–10 (2009).
  25. P. Heher, S. Mühleder, R. Mittermayr, H. Redl, P. Slezak, Fibrin-based delivery strategies for acute and chronic wound healing. *Adv. Drug Deliv. Rev.* **129**, 134–147 (2018).
  26. A. J. Hanson, M. T. Quinn, Effect of fibrin sealant composition on human neutrophil chemotaxis. *J. Biomed. Mater. Res.* **61**, 474–481 (2002).
  27. J. Vera, B. Savoldo, S. Vigouroux, E. Biagi, M. Pule, C. Rossig, J. Wu, H. E. Heslop, C. M. Rooney, M. K. Brenner, G. Dotti, T lymphocytes redirected against the  $\kappa$  light chain of human immunoglobulin efficiently kill mature B lymphocyte-derived malignant cells. *Blood* **108**, 3890–3897 (2006).
  28. Y. Xu, M. Zhang, C. A. Ramos, A. Duret, E. Liu, O. Dakhova, H. Liu, C. J. Creighton, A. P. Gee, H. E. Heslop, C. M. Rooney, B. Savoldo, G. Dotti, Closely related T-memory stem cells correlate with in vivo expansion of CAR.CD19-T cells and are preserved by IL-7 and IL-15. *Blood* **123**, 3750–3759 (2014).
  29. C. A. Ramos, B. Savoldo, V. Torrano, B. Ballard, H. Zhang, O. Dakhova, E. Liu, G. Carrum, R. T. Kamble, A. P. Gee, Z. Mei, M. F. Wu, H. Liu, B. Grilley, C. M. Rooney, M. K. Brenner, H. E. Heslop, G. Dotti, Clinical responses with T lymphocytes targeting malignancy-associated  $\kappa$  light chains. *J. Clin. Invest.* **126**, 2588–2596 (2016).
  30. S. Pellegatta, B. Savoldo, N. Di Ianni, C. Corbetta, Y. Chen, M. Patané, C. Sun, B. Pollo, S. Ferrone, F. DiMeo, G. Finocchiaro, G. Dotti, Constitutive and TNF $\alpha$ -inducible expression of chondroitin sulfate proteoglycan 4 in glioblastoma and neurospheres: Implications for CAR-T cell therapy. *Sci. Transl. Med.* **10**, eaa02731 (2018).

**Acknowledgments:** We acknowledge A. Brown at North Carolina State University for providing the MFP-3D-BIO, Asylum Research AFM equipment. **Funding:** The Microscopy Services Laboratory, Department of Pathology and Laboratory Medicine, is supported, in part, by the P30 CA016086 Cancer Center Core Support Grant to the UNC Lineberger Comprehensive Cancer Center. In addition, the research reported in this work was supported by the National Cancer Institute of Health under award numbers T32CA196689 (E.A.O.) and R25NS094093 (E.A.O.) and by the Alfred P. Sloan Foundation SSMN Grant (E.A.O.), by R21-CA229938-01A1 (G.D.), and by U01CA239258 (B.S.). **Author contributions:** Conception and design: E.A.O., Z.G., F.S.L., S.H., and G.D. Development of methodology: E.A.O., A.V., M.Y., E.L., H.H., H.D., S.K., Z.G., B.S., F.S.L., S.H., and G.D. E.A.O., A.V., M.Y., E.L., S.N., H.H., and H.D. conducted the experiments and analyzed the data. S.K., Z.G., B.S., F.S.L., S.H., and G.D. supervised the experimental design. E.A.O. and G.D. wrote the manuscript that was edited and approved by all authors. **Competing interests:** G.D., B.S., and H.D. hold patents in T cell engineering. G.D. serves on the scientific advisory board of Bellicum Pharmaceuticals and Catamaran. B.S. and G.D. are consultants for Tessa Therapeutics. Z.G. is the scientific cofounder of ZenCapsule, Zcapsule, and Zenomics. The other authors declare that they have no competing interests. **Data and materials availability:** All data needed to evaluate the conclusions in the paper are present in the paper and/or the Supplementary Materials.

Submitted 18 January 2021

Accepted 16 August 2021

Published 6 October 2021

10.1126/sciadv.abg5841

**Citation:** E. A. Ogunnaike, A. Valdivia, M. Yazdimamaghani, E. Leon, S. Nandi, H. Hudson, H. Du, S. Khagi, Z. Gu, B. Savoldo, F. S. Ligler, S. Hingtgen, G. Dotti, Fibrin gel enhances the antitumor effects of chimeric antigen receptor T cells in glioblastoma. *Sci. Adv.* **7**, eabg5841 (2021).